Journal of Chromatography Open 2 (2022) 100030

Contents lists available at ScienceDirect

Journal of Chromatography Open

journal homepage: www.elsevier.com/locate/jcoa

Original Research Article

Exploring interaction modes between polysaccharide-based selectors and biologically active 4,4′-bipyridines by experimental and computational analysis

Roberto Dallocchio[a,1], Alessandro Dessì[a,1], Barbara Sechi[a,1], Bezhan Chankvetadze[b], Sergio Cossu[c], Victor Mamane[d,*], Emmanuel Aubert[e], Carla Rozzo[f], Giuseppe Palmieri[f], Ylenia Spissu[g], Paola Peluso[a,**]

[a] Istituto di Chimica Biomolecolare ICB, CNR, Sede secondaria di Sassari, Traversa La Crucca 3, I-07100 Li Punti - Sassari, Italy
[b] Institute of Physical and Analytical Chemistry, School of Exact and Natural Sciences, Tbilisi State University, Tbilisi, Georgia
[c] Dipartimento di Scienze Molecolari e Nanosistemi DSMN, Università Ca' Foscari di Venezia, Via Torino 155, I-30172 Mestre Venezia, Italy
[d] Institut de Chimie de Strasbourg, UMR CNRS 7177, Equipe LASYROC, 1 rue Blaise Pascal, 67008 Strasbourg Cedex, France
[e] Université de Lorraine, CNRS, CRM2, F-54000 Nancy, France
[f] Unit of Cancer Genetics, Institute of Genetic and Biomedical Research IRGB, CNR, Traversa La Crucca 3, I-07100 Li Punti - Sassari, Italy
[g] ISPA CNR, Sede secondaria di Sassari, Traversa La Crucca 3, Regione Baldinca, I-07100 Li Punti - Sassari, Italy

ARTICLE INFO

Keywords:
Bipyridines
Electrostatic potential
Enantioseparation
High-performance liquid chromatography
Molecular dynamics
Polysaccharide-based chiral stationary phases

ABSTRACT

In the last few years, chiral 4,4′-bipyridine derivatives have been developed for different applications in catalysis, enantioseparation science, supramolecular and theoretical chemistry by modulating the activity of the molecular system through the introduction of specific substituents in the heteroaromatic scaffold. More recently, the biological activity of 2′-substituted-3,3′,5,5′-tetrachloro-2-iodo-4,4′-bipyridines has been explored in the field of transthyretin (TTR) fibrillogenesis inhibition, and the anticancer cytotoxicity of some derivatives is currently under systematic investigation. In this frame, the high-performance liquid chromatography (HPLC) enantioseparation of four atropisomeric 2,2′-disubstituted-4,4′-bipyridines (R, R' = Ar, I), which contain multiple interaction sites, such as hydrogen bonding (HB) donors and acceptors, halogen bond (XB) donors, and π-extended electronic clouds, was explored by using *n*-hexane (Hex)/2-propanol (2-PrOH) 90:10 v/v as a mobile phase (MP), and eight chiral columns with coated and immobilized amylose- and cellulose-based selectors. The impact of subtle structural variations of analytes and selectors on their mutual intermolecular interactivity was evaluated in terms of retention (k) and selectivity (α) factors. On this basis, chromatographic analysis based on systematic screening of analytes and selectors was integrated with electrostatic potential (V) analysis and molecular dynamics (MD) simulations as computational techniques. The effect of temperature on retention, selectivity, and enantiomer elution order (EEO) of the analytes with coated and immobilized amylose *tris*(3,5-dimethylphenylcarbamate) was also considered by comparing the variation of the thermodynamic profile associated with each enantioseparation. Chromatographic responses proved to be strictly dependent on specific regions within the analyte, and functions of different interactions sites of the analytes as the structure of the chiral selector changes were significantly disclosed.

1. Introduction

In cellulose and amylose carbamate-based polymers, two main structural features contribute to the extreme versatility of this class of chiral selectors: a) the polysaccharide backbone, where conformational chirality depends on the peculiar helical twist generated by specific glycosidic linkages forming the polymeric chain; b) the pendant groups which allow for the radial expansion of the polymer and the forma-

* Institut de Chimie de Strasbourg, UMR CNRS 7177, Equipe LASYROC, 1 rue Blaise Pascal, 67008 Strasbourg Cedes, France.
** Corresponding author at: Consiglio Nazionale delle Ricerche, Istituto di Chimica Biomolecolare Consiglio Nazionale delle Ricerche Sede di Sassari, Traversa La Crucca, 3 - Reg. Baldinca, Sassari, Italy.
E-mail addresses: vmamane@unistra.fr (V. Mamane), paola.peluso@cnr.it (P. Peluso).
[1] These authors contributed equally to this work.

https://doi.org/10.1016/j.jcoa.2022.100030
Received 30 November 2021; Received in revised form 5 January 2022; Accepted 6 January 2022
2772-3917/© 2022 The Author(s). Published by Elsevier B.V. This is an open access article under the CC BY-NC-ND license (http://creativecommons.org/licenses/by-nc-nd/4.0/)

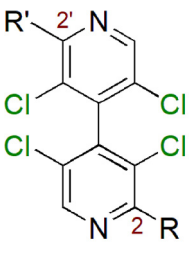

R	R'	
I	(*p*-OH)C_6H_4	(**1a**)
I	4-pyridyl	(**1b**)
4-pyridyl	(*p*-OH)C_6H_4	(**1c**)
4-pyridyl	(*p*-$OSiMe_2$*t*Bu)C_6H_4	(**1d**)
I	Ph	(**1e**)

Fig. 1. Structures of 4,4′-bipyridines **1a-e**.

tion of a chiral groove. The latter consists of a polar layer, containing the carbamate groups located inside the groove and able to exert polar interactions, and a hydrophobic layer containing substituted (R = Me, Cl) aromatic rings located outside the polymer groove and able to exert π-π and hydrophobic interactions [1,2]. Depending on type and position of the substituents on these terminal aromatic rings, several noncovalent interactions can potentially occur over the polysaccharide surface underlying selector-selectand complex formation but, as a matter of fact, only some of them act to recognize the enantiomers of a given chiral compound depending on its particular structure, size and shape. In addition, the type of noncovalent interactions determining the affinity of selectand toward the polymer can be significantly tuned by changing the mobile phase (MP), given the possibility to operate with alkane/alcohol mixtures, polar organic (PO) solvents, and aqueous organic mixtures [3]. In this molecular environment, unexplored analytes are privileged tools to profile new interaction modes and gain new information on chromatographic enantiorecognition. In turn, the information gained on the interaction capability of new analytes by using polysaccharide carbamate-based platforms in chromatography may be useful beyond the boundaries of chromatography itself in order to guide toward applications of the analytes in fields other than enantioseparation science.

Previous studies have demonstrated that functions and applications of atropisomeric 4,4′-bipyridines in catalysis [4], enantioseparation science [5–7], supramolecular [8,9], and theoretical [10] chemistry can be determined by introducing suitable functional groups in the heteroaromatic scaffold in order to tune steric and electronic properties of the molecular system. Very recently, the enantioseparation of atropisomeric 2′-substituted-3,3′,5,5′-tetrachloro-2-iodo-4,4′-bipyridines **1a, 1b** and **1e** (Fig. 1) on some polysaccharide-based chiral stationary phases (CSPs) has been reported [11,12], observing that the chromatographic response of the analytes, in terms of retention and selectivity factors, is strictly dependent on the stereoelectronic features of the distinctive substituents located at the 2,2′-positions of the 4,4′-bipyridyl core. For this class of compounds, the information about noncovalent interactivity gained by integrating chromatographic and computational analysis (Fig. 2a) [11,12] guided us toward the design and development of *a)* new inhibitors of transthyretin (TTR) misfolding, which is implicated in TTR amyloidosis diseases [13], and *b)* compounds which have been showing interesting anticancer cytotoxicity [14]. Indeed, through molecular docking simulations, compounds **1a-c** showed to fit the T_4 cavity of TTR with binding energy ranging from −7.02 to −7.26 kcal/mol (Fig. 2b), the inhibition ability being confirmed *in vitro* for compound **1a** and **1b**, and the *M*-enantiomer showing higher activity compared to the *P*-enantiomer [13]. More recently, compound **1a** (R = I, R' = HOC_6H_4) showed hydrogen bonding (HB)-driven anticancer cytotoxicity (0% cell growth at 100 μM) higher compared to compound **1e** (R = I, R' = Ph), over 48 hrs incubation time with the human metastatic $BRAF^{V600E}$-mutated melanoma cell line A375 (CRL-1619, ATCC), which is poorly responsive to conventional chemotherapeutic agent and sensitive to BRAF inhibitors (BRAFi) (Fig. 2c) [14].

Given the applicative interest of chiral 4,4′-bipyridines **1**, the enantioseparations of compounds **1c** and **1d** (Fig. 1), which contain multiple interaction sites, and **1a** and **1b**, used as reference compounds for comparison, were studied by using eight chiral columns with coated and immobilized amylose- and cellulose-based selectors. The impact of subtle structural variations of both analytes and selectors on the intermolecular interactivity underlying retention and diastereomeric complex formation was explored by integrating chromatographic analysis, based on systematic screening of analytes and selectors, and electrostatic potential (V) analysis and molecular dynamics (MD) simulations as computational techniques. Finally, the effect of temperature on the enantioseparation of 4,4′-bipyridines **1c** and **1d** with coated and immobilized amylose *tris*(3,5-dimethylphenylcarbamate) (ADMPC) were evaluated and compared with the thermodynamic profiles of the recently described iodinated analogues **1a** and **1b** [11].

2. Experimental

2.1. Chemicals

Compounds **1a-d** were synthesized and characterized as reported earlier [13,15].

2.2. Chromatography

An Agilent Technologies (Waldbronn, Germany) 1100 Series HPLC system (high-pressure binary gradient system equipped with a diode-array detector operating at multiple wavelengths (220, 254, 280, 360 nm), a programmable autosampler with a 20 μl loop, and a thermostated column compartment) was employed for both analytical and multimilligram separations. Data acquisition and analyses were carried out with Agilent Technologies ChemStation Version B.04.03 chromatographic data software. The UV absorbance is reported as milliabsorbance units (mAU). Lux Amylose-1 and i-Amylose-1 (amylose *tris*(3,5-dimethylphenylcarbamate) (ADMPC)) (A-1 and iA1, respectively), Lux Amylose-2 (amylose *tris*(5-chloro-2-methylphenylcarbamate) (ACMPC-2)) (A-2), Lux i-Amylose-3 (amylose *tris*(3-chloro-5-methyl-phenylcarbamate) (ACMPC-3)) (iA-3), Lux Cellulose-1 (cellulose *tris*(3,5-dimethylphenylcarbamate) (CDMPC)) (C-1), Lux Cellulose-2 (cellulose *tris*(3-chloro-4-methylphenylcarbamate) CCMPC-2)) (C-2), Lux Cellulose-4 (cellulose *tris*(4-chloro-3-methylphenylcarbamate) (CCMPC-4)) (C-4), and Lux i-Cellulose-5 (cellulose *tris*(3,5-dichlorophenylcarbamate) (CDCPC)) (iC-5) were used as chiral columns (5 μm, 250 × 4.6 mm) (Phenomenex Inc., Torrance, CA, USA) (Table 1). HPLC grade *n*-hexane (Hex), 2-propanol (2-PrOH), and methanol (MeOH) were purchased from Sigma-Aldrich (Taufkirchen, Germany). Dead time (t_0) was measured by injection of tri-*tert*butylbenzene (Sigma-Aldrich) as a non-retained compound [16]. Analyses were performed in isocratic mode at 25 °C. The flow rate (FR) was set at 0.8 ml/min. For compounds **1a** and **1b**, the enantiomer elution order (EEO) was determined by injecting enantiomers of known absolute configuration [13]. Pure enantiomers of compound **1c** were obtained by HPLC enantioseparation (Supplementary material) and their absolute configuration was assigned by comparison of theoretical and experimental electronic circular dichroism (ECD) spectra (see Supplementary material for theoretical ECD details). ECD spectra of **1c** enantiomers were recorded at room temperature using 0.15 mM samples in methanol and a 1 mm quartz cell at 22 °C. For compound **1d**, the relative EEO was assigned by injecting pure enantiomers of unknown absolute configuration which are denoted as X and Y. The separations at various temperature were conducted at 10, 15, 20, 25, 30, 35, 40, and 45 °C in a thermostated column chamber equipped with a RE104 LAUDA circulating water-bath (Lauda, Königshofen, Germany). When the temperature was changed, the column was allowed to equilibrate for 1 h before injecting the samples. Thermodynamic parameters were derived from the slopes (ΔH and $\Delta\Delta H$) and the intercepts ($\Delta S^* = \Delta S/R + \ln\Phi$ and $\Delta\Delta S$) of the van't Hoff plots by

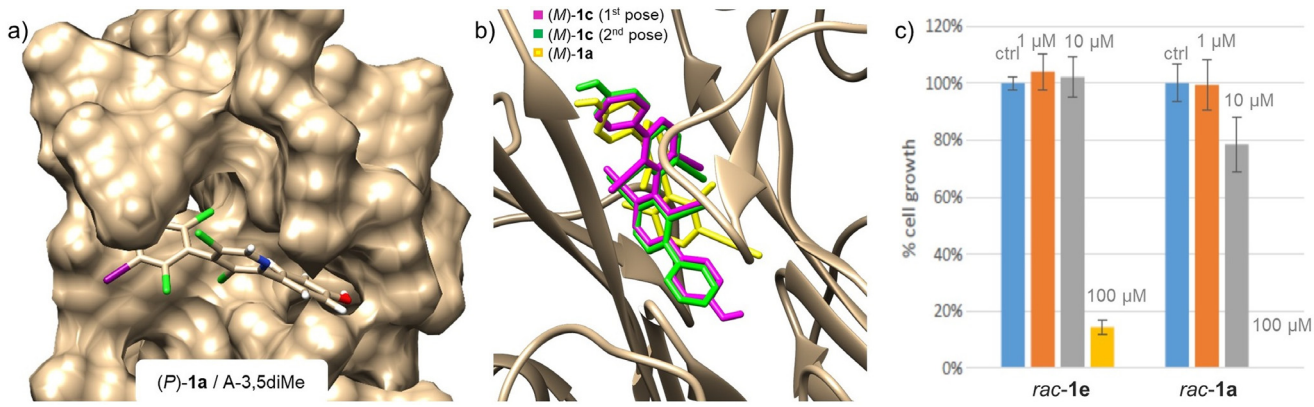

Fig. 2. a) Representative snapshot from the simulated MD trajectories of (*P*)–**1a** complex with amylose *tris*(3,5-dimethylphenylcarbamate) [12]; b) docking modes into the T_4 binding pocket for the (*M*)-enantiomers of **1a** (yellow) [13] and **1c** (pink, green) (superimposed structures); c) anticancer cytotoxicity of *rac*-**1a** and *rac*-**1e** observed at variable concentration of ligand after 48 hrs incubation with A375 melanoma cell line [14].

Table 1
Chiral columns and selectors used for the enantioseparations of compounds **1a-d**.

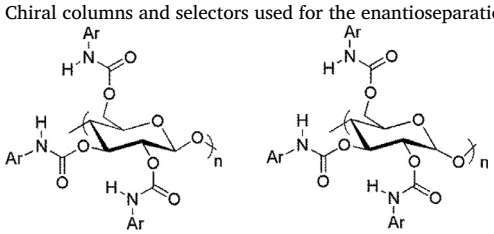

Column[a] Name	Type	Acronym	Chiral selector Name	Acronym
Cellulose-1	coated	C-1	cellulose *tris*(3,5-dimethylphenylcarbamate)	CDMPC
Cellulose-2	coated	C-2	cellulose *tris*(3-chloro-4-methylphenylcarbamate)	CCMPC-2
Cellulose-4	coated	C-4	cellulose *tris*(4-chloro-3-methylphenylcarbamate)	CCMPC-4
i-Cellulose-5	immobilized	iC-5	cellulose *tris*(3,5-dichlorophenylcarbamate)	CDCPC
Amylose-1	coated	A-1	amylose *tris*(3,5-dimethylphenylcarbamate)	ADMPC
i-Amylose-1	immobilized	iA-1	amylose *tris*(3,5-dimethylphenylcarbamate)	ADMPC
Amylose-2	coated	A-2	amylose *tris*(5-chloro-2-methylphenylcarbamate)	ACMPC-2
i-Amyose-3	immobilized	iA-3	amylose *tris*(3-chloro-5-methylphenylcarbamate)	ACMPC-3

[a] Lux series columns (Phenomenex).

linear regression analysis. *R* is the gas constant (1.987 cal•K^{-1}mol^{-1}) and Φ is the phase ratio of the column. Statgraphics Centurion XVI (Statpoint Technologies, Inc., Warrenton, VA, USA) was used for all linear regression analyses.

2.3. Computationals

The 3D structures of compounds **1a-d** and methyl 3,5-dimethylphenylcarbamate, methyl 3-chloro-4-methylphenylcarbamate, methyl 4-chloro-3-methylphenylcarbamate, methyl 3,5-dichloromethylphenylcarbamate, methyl 3-chloro-5-methylcarbamate, and methyl 5-chloro-2-methylphenylcarbamate, as frameworks representing the selector pendant groups, were prepared using the build function, and model kits and tools provided by Spartan' 10 Version 1.1.0 (Wavefunction Inc., Irvine, CA, USA) [17] for building and editing organic molecules. Geometry optimization and computation of electrostatic potential isosurfaces (V_S) and related parameters (V_S extrema, $V_{S,max}$ and $V_{S,min}$ values, given in au) were performed by using Gaussian 09 at density functional theory (DFT) level (B3LYP, 6–311G*) (Wallingford, CT 06,492, USA) [18]. Search for the exact location of such $V_{S,max}$ and $V_{S,min}$ was made through the Multiwfn code [19] and through its module enabling quantitative analyses of molecular surfaces (isovalue 0.002) [20]. The AMBER18 software [21] was used to carry out 100 ns MD simulations, and the Chimera software (UCSF, San Francisco, USA) was used for visualization and analysis of the MD trajectories [22]. MD details are reported as Supplementary material.

3. Results and discussion

3.1. Analyte structures

All compounds **1a-d** contain a common 3,3′,5,5′-tetrachlorinated motif that represents a symmetric hydrophobic region surrounding the chiral axis. Otherwise, distinctive substituents are located at 2,2′-positions, which present an orthogonal-like orientation. Due to the atropisomeric topology of 3,3′,5,5′-tetrachloro-4,4′-bipyridines **1a-d**, it was expected that the enantiodifferentiation degree would be dependent on the type of interaction sites located at both 2- and 2′-positions, and on the strength of noncovalent interactions between these sites and those featuring the polymeric selectors used in this study. Thus, for compounds **1a-d**, $V_{S,max}$ (Table 2, pale blue points) and $V_{S,min}$ (red points) values were computed at DFT level of theory in order to inspect the effect

Table 2
Calculated $V_{S,max}$ (pale blue) and $V_{S,min}$ (red) (au) on a 0.002 au isosurface for 3,3′,5,5′-tetrachloro-4,4′-biyridines **1a-d** (DFT/B3LYP/6–311G*).

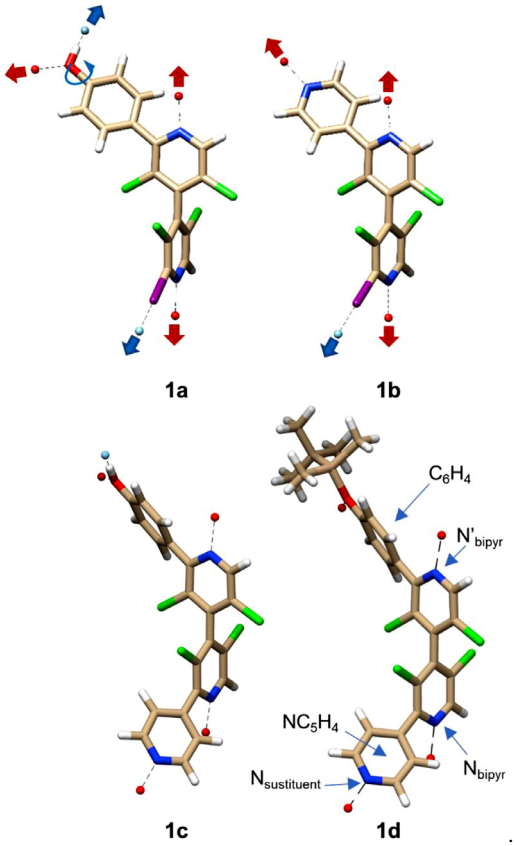

Descriptor	1a	1b	1c	1d
		$V_{S,min}$		
O<u>H</u>	−0.0421		−0.0420	−0.0273
N_{bipyr}	−0.0490	−0.0450	−0.0469	−0.0479
N'_{bipyr}	−0.0489	−0.0428	−0.0494	−0.0509
$N_{substituent}$		−0.0659	−0.0684	−0.0690
C_6H_4 π-cloud	−0.0205		−0.0203	−0.0230
NC_5H_4 π-cloud		−0.0087	−0.0126	−0.0119
		$V_{S,max}$		
2-I	0.0496	0.0532		
O<u>H</u>	0.1128		0.1128	

of subtle structural variations on the electron charge density distribution associated to the main electron-poor (electrophile, Lewis acid) and electron-rich (nucleophile, Lewis base) recognition sites, respectively (Table 2). When two molecules approach each other, the tendency will be that the regions of positive V on a molecule are attracted to those of negative V on another molecule. Based on this concept, recently V analysis has been fruitfully used to gain insights on molecular contacts by evaluating the electron charge density on molecular regions involved in noncovalent interactions [23,24].

Compounds **1c** and **1d** contain a π-extended electronic system consisting of four connected aromatic rings. Moreover, HB sites are present on the substituents located at the 2,2′-positions: *a)* a HB acceptor site ($N_{substituent}$) ($V_{S,min}$ = –0.0684 and –0.0690, respectively) located on the 4-pyridyl group at the 2-position in both compounds, *b)* HB donor (O<u>H</u>) ($V_{S,max}$ = 0.1128 au) and acceptor (<u>O</u>H) ($V_{S,min}$ = –0.0420 au) sites located on the hydroxyl group at the 2′-position in **1c**, and *c)* a HB acceptor site (<u>O</u>SiR_3) ($V_{S,min}$ = –0.0777 au) located on the *t*$BuMe_2SiO$ moiety at the 2′-position in compound **1d**. As the OH group in **1a** and **1c** is free to rotate around the C–O bond, the directionality of the HB sites involving the OH may change, in principle making the 4-hydroxyphenyl group more adaptable to the CSP chiral cavities than the 4-pyridyl. In the latter case, the rotation of the 4-pyridyl substituent does not change the directionality of the HB involving the pyridyl nitrogen. Likely for this reason, **1a** has shown to be more efficient than **1b** with different synthetic [11,12] and biological [13,14] receptors, in terms of binding and function. Compound **1c** presents the same values of V extrema on the sites located on the 4-hydroxyphenyl group at the 2′-position ($V_{S,max}$ (O<u>H</u>) = 0.1128 au; $V_{S,min}$ (<u>O</u>H) = –0.0420 au; $V_{S,min}$ (C_6H_4 π-cloud) = –0.0203 au) compared to compound **1a** ($V_{S,max}$ (O<u>H</u>) = 0.1128 au; $V_{S,min}$ (<u>O</u>H) = –0.0421 au; $V_{S,min}$ (C_6H_4 π-cloud) = –0.0205 au), revealing that changing the iodine atom to the 4-pyridyl, at the 2-position, does not affect the electronic properties at the 2′-position. In compound **1c**, the electron charge density on the 4-pyridyl moiety at the 2-position ($V_{S,min}$ ($N_{substituent}$) = –0.0684 au; $V_{S,min}$ (NC_5H_4 π-cloud) = –0.0126 au) increases slightly compared to **1b** ($V_{S,min}$ ($N_{substituent}$) = –0.0659 au; $V_{S,min}$ (NC_5H_4 π-cloud) = –0.0087 au). In compound **1d**, the presence of the *t*$BuMe_2SiO$ moiety in place of the H in the substituent at the 2′-position has the effect of removing the HB donor site that is present in **1c**, and of increasing the electron charge density on both oxygen and π-electronic cloud (**1d**: $V_{S,min}$ (<u>O</u>SiR_3) = –0.0777 au; $V_{S,min}$ (C_6H_4 π-cloud) = –0.0230 au) compared to **1a** ($V_{S,min}$ (C_6H_4 π-cloud) = –0.0205 au) and **1c** ($V_{S,min}$ (C_6H_4 π-cloud) = –0.0203 au). As already reported [11,12], both compounds **1a** and **1b** contain an iodine atom as substituent at the 2-position, whereas 4-pyridyl and 4-hydroxyphenyl rings are the distinctive substituents at the 2′-position, respectively. In these compounds the iodine may act as XB donor interacting through its electrophilic σ-hole with the nucleophilic regions of the polymeric selector. Previous studies showed that a XB interaction actually drives enantioseparation of **1b** on C-1, by using Hex-containing mixtures as MPs. Indeed, higher polarization was induced by the 4-pyridyl substituent ($V_{S,max}$ (I) = 0.0535 au) on the 2-iodine compared to the 4-hydroxyphenyl substituent ($V_{S,max}$ (I) = 0.0496 au).

3.2. Polysaccharide-based selectors

C-1, C-2, C-4, iC-5, A-1, iA-1, A-2 and iA3 as chiral columns (Table 1) were selected for this study in order to evaluate the impact of aryl chlorination and covalent immobilization on the enantioseparation performances of the corresponding CSPs toward *rac*-**1c** and *rac*-**1d**, using **1a** and **1b** as reference compounds of comparison. All columns contain selectors based on cellulose and amylose backbones which are derivatized with distinctive pendant groups determining the stereoelectronic properties of each selector. In this context, three key regions of the pendant groups strongly contribute to retention and selectivity, namely the electrophilic amidic hydrogen (N-H), the nucleophilic carbonyl oxygen (C=O) and the π-electronic cloud. To quantify the effect of type and position of the substituents of the terminal aromatic rings on the electron charge density of the pivotal components of each pendant group, $V_{S,max}$ (Table 3, pale blue point) and $V_{S,min}$ (red point) values were also computed at DFT level of theory (Table 3). Calculating V extrema confirmed that introducing chlorine modifies the electron density distribution on the pendant group moiety, thus the electron density on both C=<u>O</u> and phenyl ring decreases (π-acidity increases), and the acidity of the N–<u>H</u> increases. In previous studies, it was observed through IR analyses that the introduction of chlorine increases the fraction of free N-H groups available for intermolecular interactions between selector and selectand [25,26]. In the meantime, the fraction of N-H involved in intramolecular HBs, contributing to maintain the high-ordered structure of the CSP, decreases. This could produce for the chlorinated CSPs a wider cavity available for the enantiomers with respect to the dimethylated selectors, the enantioseparation resulting from the balance of carbamate polarity and intramolecular HB ability [25,26].

Table 3
$V_{S,max}$ and $V_{S,min}$ values (a.u.) associated with the main recognition sites (carbamate N-H, C=O, and Ar) of cellulose- and amylose-based selectors used in the study (DFT/B3LYP/6–311G*).

Chiral selector	Side chain	Descriptors	$V_{S,max}$ (N-H)	$V_{S,min}$ (C=O)	$V_{S,min}$ (Ar)
CDMPC/ADMPC	3,5-dimethylphenylcarbamate		0.0843	−0.0625	−0.0271
CCMPC-2	3-chloro-4-methylphenylcarbamate		0.0911	−0.0578	−0.0165
CCMPC-4	4-chloro-3-methylphenylcarbamate		0.0919	−0.0580	−0.0165
CDCPC	3,5-dichlorophenylcarbamate		0.0990	−0.0536	−0.0066
ACMPC-2	5-chloro-2-methylphenylcarbamate		0.0853	−0.0588	−0.0179
ACMPC-3	3-chloro-5-methylphenylcarbamate		0.0914	−0.0595	−0.0163

3.3. Chromatographic screening with n-hexane/2-propanol 90:10 as a mobile phase

In the first step of this study, *rac*-**1c** was enantioseparated at multimilligram scale (>99% ee) on iA-3 by using Hex/2-PrOH 85:15 v/v as a MP (Supplementary material, Table S1). The absolute configuration of HPLC-separated enantiomers of bipyridine **1c** was determined by comparing the measured ECD spectra (Supplementary material, Fig. S1) with the one calculated by time-dependent DFT (TD-DFT) calculations for the (*M*) enantiomer. The calculation of the ECD spectrum was performed considering all the possible conformers arising from the rotation of the substituents in the 2- and 2′-positions with respect to the bipyridine rings (Supplementary material, section S3 for details). A good match was obtained with the spectrum of the second eluted enantiomer, allowing unambiguous absolute configuration assignment (Supplementary material, Fig. S2).

Then, the enantioseparation of 4,4′-bipyridines **1a-d** was explored on the eight polysaccharide-based CSPs by using Hex/2-PrOH 90:10 as MP (Table 4), which was expected to favor and stabilize HB and other polar interactions. For compound **1d**, the relative EEO was assigned by injecting pure enantiomers of unknown absolute configuration which are denoted as *X* and *Y*. In this case, it was not possible to determine the absolute configuration of the collected enantiomers due to limited amounts of the available material. However, given that a common *P-M, P-M, P-M, X-Y* pattern was obtained for the EEO of compounds **1a-d**, respectively, on iC-5 and A-2, it appeared reasonable to also assign $X = P$ and $Y = M$ for compound **1d**

By integrating the results of the chromatographic screening, which are summarized in Table 4, and *V* values associated to the main interaction sites of analytes and selectors, the following remarks emerged:

i) retention factors of compounds **1b-d** showed to be higher on the chlorinated selectors ($1.55 \leq k_1 \leq 17.25$), which contain better HB donor sites (N–H) compared to the methylated selectors ($0.83 \leq k_1 \leq 13.53$). This confirmed that the interaction between the pyridyl nitrogen on the analytes and the amidic hydrogen on the CSPs drives retention. In addition, for compound **1a**, higher retention factors on the methylated selectors were obtained ($2.94 \leq k_1 \leq 6.28$) compared to the chlorinated polymers ($1.38 \leq k_1 \leq 3.35$), showing a pivotal role of the intermolecular HB between the hydroxyl hydrogen of the analyte and the carbonyl oxygen of the selector;

ii) the highest enantioselectivity values were obtained for all compounds on the methylated selectors with selectivity factors ranging from 1.26 to 2.83. However good selectivity values were also provided by the chlorinated iA-3 in the case of **1c** and **1d** (α = 1.31 and 1.23, respectively);

iii) in most cases, EEO was observed to be *P-M*. In previous study, backbone-dependent EEO reversal was reported for compounds **1a** and **1b** by changing CDMPC (*P-M*) to ADMPC (*M-P*). It is interesting to note that an analyte-dependent EEO reversal also occurred moving from **1a** and **1b** (*M-P*) to compounds **1c** and **1d** (*P-M*) on ADMPC. In this study, pendant group-dependent EEO reversals were also obtained by changing CDMPC (*P-M*) to CCMPC-2 (*M-P*) for **1a**, and CDMPC (*P-M*) to CCMPC-4 (*M-P*) for **1b**. Otherwise, compound **1c** retained the same EEO (*P-M*) on both ADMPC and CCMPC-4;

iv) the iodine substituent at the 2-position in **1a** and **1b** has a pivotal role on C-1 (α = 1.14 and 2.83, respectively) when mixture A is used as a MP, because changing it to the 4-pyridyl group (**1a**→**1c**), to

Table 4
Chromatographic conditions, parameters and EEOs for the enantioseparations of **1a-d** on polysaccharide-based CSPs (MP = Hex/2-PrOH 90:10 v/v (A), MeOH (B), *FR* = 0.8 ml/min, *T* = 25 °C).

CSP	MP	t_1 [min]	t_2 [min]	k_1	k_2	α	EEO
			1a				
C-1	A	13.97	15.39	2.94	3.35	1.14	*P-M*
C-1	B	6.40	6.40	0.59	0.59	1.00	–
iC-5	A	9.26	10.07	1.38	1.59	1.15	*P-M*
C-2	A	11.01	11.51	2.07	2.21	1.07	*M-P*
C-4	A	11.24	11.24	2.03	2.03	1.00	–
A-1	A	25.50	31.31	6.28	7.93	1.26	*M-P*
iA-1	A	21.56	21.56	4.97	4.97	1.00	–
A-2	A	16.23	17.30	3.35	3.73	1.09	*P-M*
iA-3	A	13.11	13.76	2.61	2.79	1.07	*P-M*
			1b				
C-1	A	12.97	30.25	2.66	7.54	2.83	*P-M*
C-1	B	8.11	8.11	1.01	1.01	1.00	–
iC-5	A	30.65	33.41	6.89	7.58	1.10	*P-M*
C-2	A	20.72	20.72	4.78	4.78	1.00	–
C-4	A	21.02	22.87	4.66	5.16	1.11	*M-P*
A-1	A	14.02	14.42	3.00	3.12	1.04	*M-P*
iA-1	A	12.91	13.74	2.58	2.80	1.09	*P-M*
A-2	A	20.21	21.11	4.52	4.77	1.05	*P-M*
iA-3	A	16.39	16.39	3.51	3.51	1.00	–
			1c				
C-1	A	28.68	28.68	6.96	6.96	1.00	–
C-1	B	5.96	6.24	0.48	0.55	1.14	*P-M*
iC-5	A	66.19	73.95	17.25	19.39	1.12	*P-M*
C-2	A	64.31	64.31	17.08	17.08	1.00	–
C-4	A	67.94	74.34	16.76	18.42	1.10	*P-M*
A-1	A	49.18	60.74	13.53	16.95	1.25	*P-M*
iA-1	A	34.70	45.26	8.74	11.71	1.34	*P-M*
A-2	A	44.96	46.38	11.20	11.59	1.03	*P-M*
iA-3	A	41.46	52.99	10.32	13.47	1.31	*P-M*
			1d				
C-1	A	6.58	6.58	0.83	0.83	1.00	–
C-1	B	7.13	7.41	0.77	0.84	1.09	*X-Y*
iC-5	A	20.14	21.59	4.55	4.95	1.09	*X-Y*
C-2	A	9.06	9.95	1.55	1.80	1.16	*X-Y*
C-4	A	10.26	11.56	1.68	2.02	1.20	*X-Y*
A-1	A	7.48	9.54	1.21	1.82	1.50	*X-Y*
iA-1	A	8.10	10.04	1.28	1.82	1.43	*X-Y*
A-2	A	10.59	11.44	1.85	2.11	1.12	*X-Y*
iA-3	A	9.95	11.40	1.72	2.11	1.23	*X-Y*

the 4-hydroxyphenyl group (**1b**→**1c**), or to the *t*BuMe$_2$SiOC$_6$H$_4$ group (**1b**→**1d**) caused loss of enantioseparation. Analogously, changing the Hex-alcohol to pure methanol with C-1 provided a dramatic drop of selectivity for **1a** and **1b**. Otherwise, under PO conditions the selectivity of **1c** and **1d** slightly increases (α = 1.14 and 1.09, respectively), likely due to the presence of the extended hydrophobic aromatic region consisting of four aromatic rings;

v) on C-1, the retention of **1c** seems to be determined by the additive contribution of the HBs arising from the two groups at the 2,2′-positions (k_1 (**1a**) + k_1 (**1b**) = 5.60 *vs* k_1 (**1c**) = 6.96). Changing the hydroxyl hydrogen to the silyl group (**1c**→**1d**) alters the stereoelectronic properties at the 2′ region with a relevant reduction of the retention factor of the first eluted enantiomer from 6.96 to 0.83. By using methanol as MP on C-1, retention of compounds **1a-d** decreased in all cases following the order **1c** < **1a** < **1d** < **1b**. Thus, slightly higher retention was obtained for compounds **1d** and **1b** featured by more acidic π-electronic clouds revealed by less negative $V_{S,min}$ values associated with the 4-pyridyl aromatic regions (–0.0119 and –0.0087 au, respectively). The π-acidic aromatic clouds may be better counterparts in π-π interactions with the π-basic 3,5-dimethylphenyl moieties of CDMPC;

vi) an interesting complementarity between C-2 and C-4 could be observed. While C-2 could enantioseparate **1a**, it was unable to resolve *rac*-**1b** and –**1c**. The opposite trend was observed on C-4 which was able to enantioseparate **1b** and **1c**, but not **1a**. This behavior showed that in **1c** the two groups at the 2,2′-position are able to contribute cooperatively to the enantioselection with the C-4, with a dominant contribution of the 4-pyridyl moiety. Otherwise with C-2, the dominant contribution of the 4-pyridyl group opposes to the interaction activity of the 4-hydroxyphenyl group, which is dominant in compound **1a**. It is interesting to note that in compound **1d** the absence of the hydroxyl oxygen had a beneficial effect on the enantioseparation, in particular with C-2.

On this basis, the two groups at 2 and 2′-positions showed to act with a positive cooperation on amylose-based chiral columns A1, iA1, and iA3, which provide higher selectivity factors for **1c** ($1.25 \leq \alpha \leq 1.34$) compared to compounds **1a** and **1b** ($1.04 \leq \alpha \leq 1.26$). Otherwise, the presence of both groups appeared to be detrimental for the enantioseparation of **1c** with system C-1/A (α = 1.00) compared to **1a** (α = 1.14) and **1b** (α = 2.83). On the contrary, the extended π-electronic system featuring **1c** exerted a beneficial effect on selectivity under PO condition (α = 1.14), compounds **1a** and **1b** being unseparated in this case. In most cases, the introduction of the silyl moiety (**1c**→**1d**) showed to be beneficial for enantioseparation, in particular on amylose-based CSP. It is likely that removing the hydroxyl oxygen, which increases the affinity of **1c** toward the selectors, allowed for more efficient modulation of the intermolecular HBs involving the 4-pyridyl group.

3.4. Effect of temperature on the enantioseparation with coated and covalently immobilized ADMPC

In a previous study, the application of van't Hoff analysis allowed for identifying different thermodynamic profiles for compounds **1a** and **1b** as the cause of the different selectivity observed by changing the coated ADMPC to the immobilized one (Fig. 3a-d) [11]. In particular, for compound **1b** a reversal of EEO was observed with coated (*M-P*) and immobilized (*P-M*) selectors. It was found that the *P-M* elution order was related to the occurrence of a hydrophobic mechanism underlying enantioselection and associated to entropic thermodynamic profiles [11]. It is worth mentioning that several studies published over time reported differences in chiral recognition ability of coated and covalently immobilized amylose-based CSP [3,27,28].

Given that for the enantioseparation of compounds **1c** and **1d** no reversal of EEO was observed on both coated and immobilized ADMPC-based columns, we also explored the impact of temperature on the enantioseparation of these compounds on the ADMPC-based columns. In particular, we aimed to confirm if the *P-M* elution order observed on ADMPC is associated with the entropic thermodynamic profiles also for compounds **1c** and **1d**. The application of van't Hoff analysis (Supplementary material for details) allows for calculating the thermodynamic parameters governing enantiomer adsorption and enantioseparation [29–31]. Despite the fact that this analysis does not allow for determining individually achiral and chiral features of enantioseparation and their actual ratio in the discrimination process [32,33], it allows for providing meaningful information on chiral recognition mechanism [11,30,31].

On this basis, retention and selectivity of compounds **1c** and **1d**, on coated A-1 and immobilized iA-1 with Hex/2-PrOH 90:10 v/v as a MP, were determined at different temperatures from 10 to 45 °C in 5 °C increments (Supplementary material, Table S2). The thermodynamic quantities derived from van't Hoff plots (Fig. 3e-h) are reported in Table S3 (Supplementary material). As hypothesized, for compounds **1c** and **1d** enantioseparation was entropy-driven in most cases:

i) for the enantioseparations of compound **1c** on coated and immobilized ADMPC, negative T_{ISO} values were calculated in both cases. However, a higher value was obtained on the coated column (−32 °C) (Fig. 3e) compared to its immobilized version (−87 °C) (Fig. 3f). On this basis, the operative temperature was higher than the determined T_{ISO}, therefore the recognition process was entropy–driven ($|T\Delta\Delta S^\circ| > |\Delta\Delta H^\circ|$) on both A-1 and iA-1. The $\Delta\Delta G^\circ$ values associated with the enantioseparation was higher for the immobilized ADMPC (−174.7 cal/mol) compared to the coated selector (−130.3 cal/mol);

ii) for the enantioseparation of compound **1d** on coated ADMPC (Fig. 3g) a more negative T_{ISO} value (−139 °C) was calculated, revealing an entropy-driven enantioseparation also in this case. Otherwise, on immobilized ADMPC (Fig. 3h), an enthalpy-driven process occurred ($|T\Delta\Delta S^\circ| < |\Delta\Delta H^\circ|$), and the difference between the free energies associated to the transfer of the enantiomers from the MP to the selector surfaces is essentially due to a negative enthalpy contribution (−119 cal/mol), whereas the entropy term is positive and close to zero (0.31 cal·K^{-1}·mol^{-1}). Indeed, the enantioselectivity is almost independent of the temperature variation (Supplementary material, Table S2). For **1d**, the $\Delta\Delta G^\circ$ values associated with the enantioseparation was higher for the coated ADMPC (−244.0 cal/mol) compared to the immobilized selector (−211.4 cal/mol), showing an opposite trend compared to that of compound **1c** [31].

The collected results confirmed that the observed EEO is dependent on the type of thermodynamic pattern, and two recognition mechanisms could be confirmed for the enantioseparation of compounds **1a-1d** on ADMPC-based columns: a) in the enthalpic domains (**1a** and **1b**), the EEO is *M-P*, likely due to HB-driven mechanisms; b) in the entropic domains, in general the EEO is *P-M*, and in this case a 'hydrophobic' mechanism driven by aryl rings and related π-π interactions controls enantioseparation. As previously reported, *P-M* was always observed as EEO for compound **1e** (*R* = I; R' = Ph), which contains a phenyl group as distinctive 2′-substituent [11]. It is worth noting that only for the enantioseparation of compound **1d** on the iA-1 the *P-M* elution order was determined under enthalpic thermodynamic conditions.

3.5. Molecular dynamics simulations

As reported in Table 4, CDMPC and ADMPC showed different enantioseparation performances toward compound **1c**, with α = 1.00 and 1.25, respectively, and *P-M* as EEO on the amylose-based selector. Moreover, on the basis of the thermodynamics experiments, a hydrophobic mechanism was hypothesized to underlie complex formation, with a relevant entropic contribution to enantioselection (thermodynamic ratio $Q = \Delta\Delta H^\circ/(298\times\Delta\Delta S^\circ$ = 0.81 (A-1) and 0.62 (iA-1). On this basis, with the aim to explore the molecular basis of these chromatographic behaviours, a theoretical investigation based on MD simulations was performed by using CDMPC and ADMPC nonamers as virtual models of the polysaccharide-based selectors. 100 ns MD simulations in the AMBER force field were performed by using the mixture Hex/2-PrOH 90:10 as a virtual solvent in accord with the experimental conditions used in

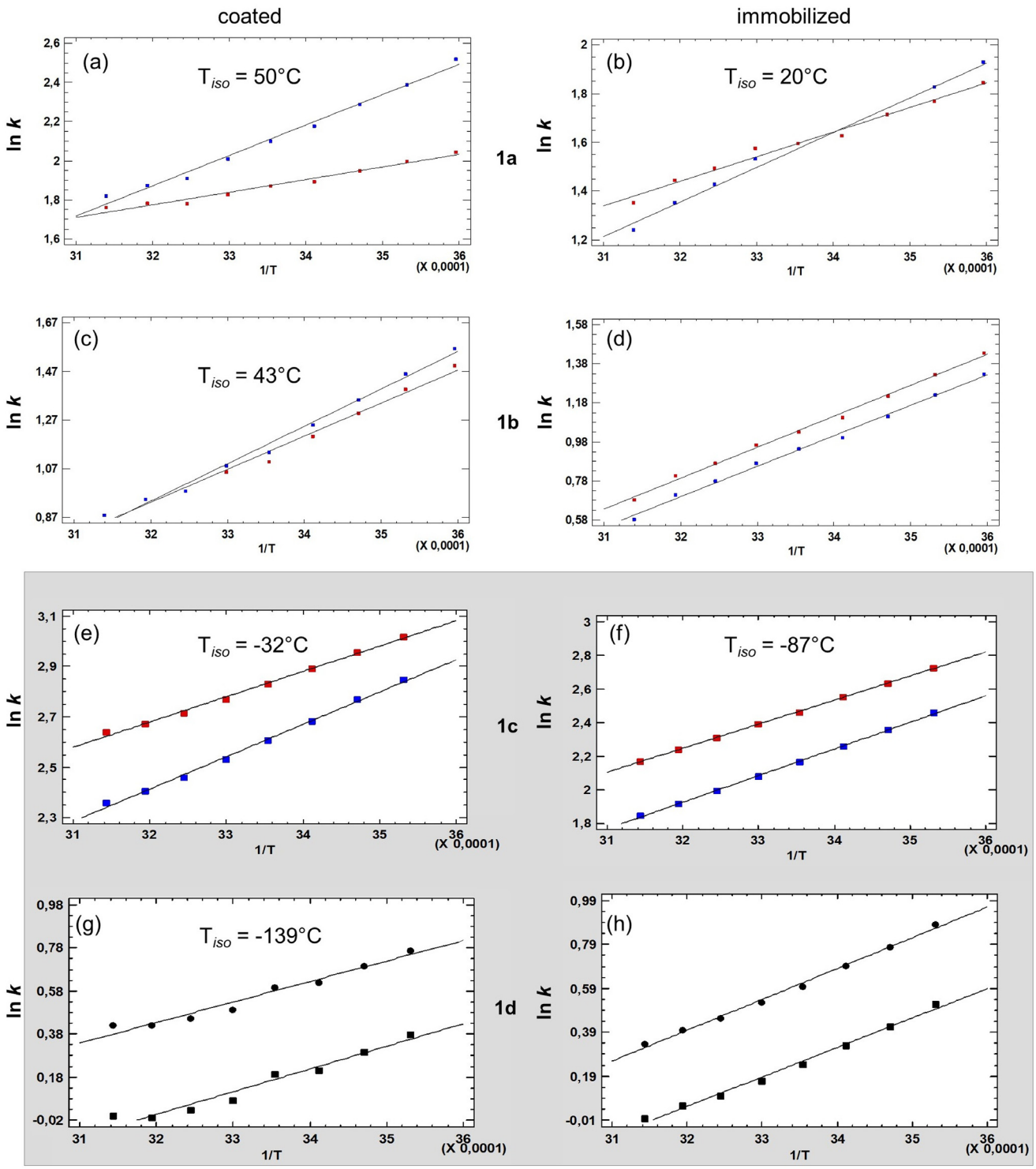

Fig. 3. ln *k* vs. 1/T plots for the enantioseparation of **1a-d** on Lux Amylose-1 and i-Amylose-1 columns (Hex/2-PrOH 90:10, 0.8 ml/min, temperature range 278.15–318.15 K for **1a** and **1b**, and 283.15–318–15 K for **1c** and **1d**; color legend: *k* (*P*), blue point, *k* (*M*), red point.

the chromatographic studies. The total interaction energies calculated for (*M*)- and (*P*)-enantiomers of **1c** in its complexes with each of the polysaccharide nonamer are reported in Figure S3 (Supplementary material) and Fig. 4 for CDMPC and ADMPC complexes, respectively. The reported energies are mean values that were calculated from 5000×3 complexes extracted by snapshots taken every 20 ps from the trajectories of three 100 ns MD replicas [34]. The interaction energy (E_{int}) between enantiomer and selector is calculated on the basis of the energies of the selector–enantiomer complex, the selector, and the enantiomer (Eq. (1))

$$E_{int} = E_{total} - E_{enantiomer} - E_{polysaccharide-based\ selector} \quad (1)$$

In Figures S3 and 4, representative snapshots and noncovalent interactions from the simulated MD trajectories of **1c** complexes with CDMPC (Fig. S3) and ADMPC (Fig. 4) are depicted. The following remarks emerged:

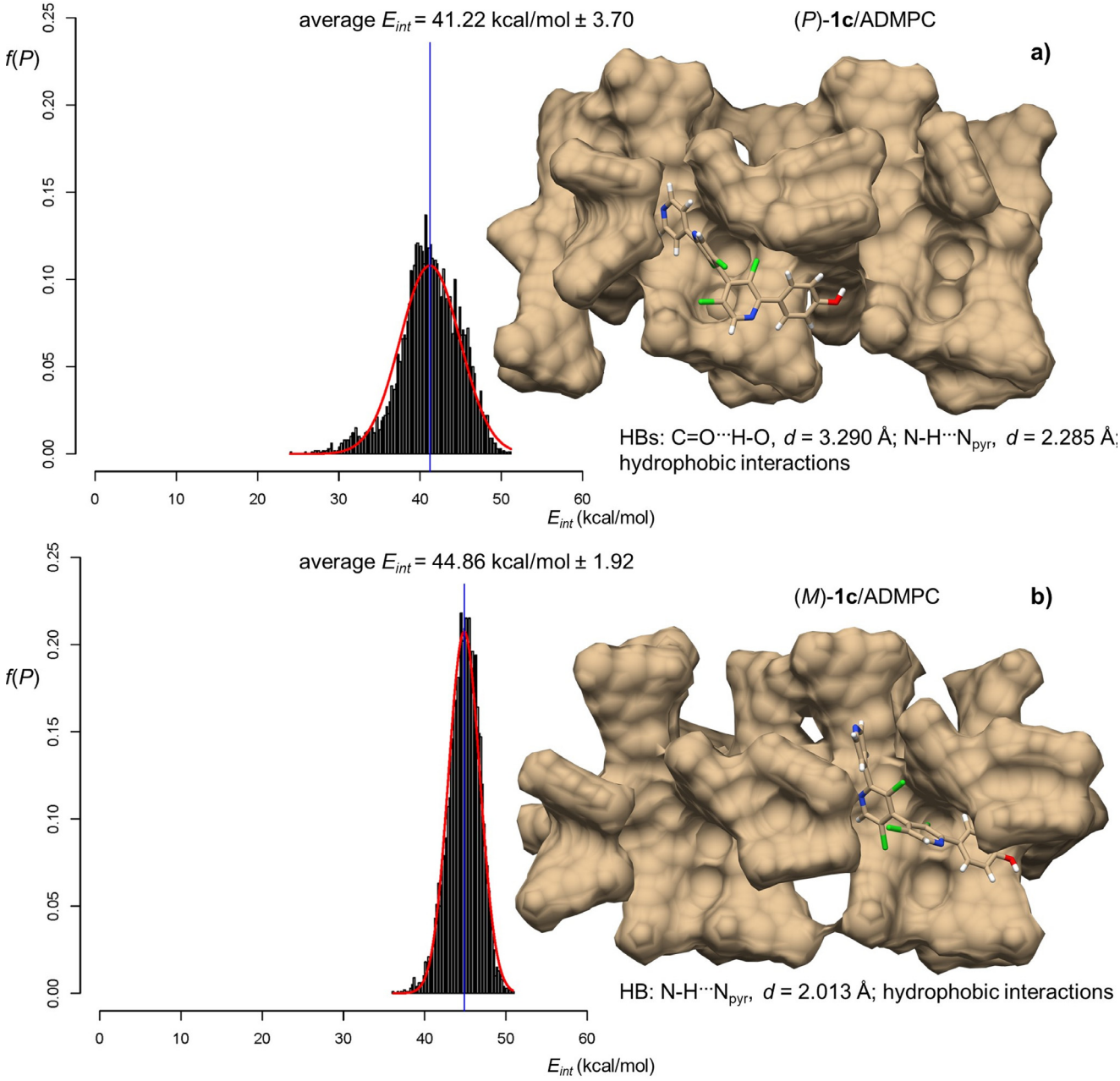

Fig. 4. Distribution of interaction energies of selector/selectand complexes over three cycles of 100 ns MDs (5000 frames/simulation), and representative snapshots from the simulated MD trajectories: a) (*P*)–**1c**/ADMPC, b) (*M*)–**1c**/ADMPC.

i) MD simulations provided a more compact structure for ADMPC compared to the CDMPC and, coherently, in CDMPC the cavities hosting the enantiomers appeared to be bigger and more exposed toward the surrounding space (Fig. S3) compared to those of ADMPC (Fig. 4);

ii) in CDMPC (Fig. S3), the two enantiomers are accommodated in the same cavity. In addition, the same type of noncovalent interactions underlies complex formation: a C=O···H–O HB with distance of 1.988 and 1.930 Å for the (*P*)- and (*M*)-complexes, respectively, and a π-π interaction involving the 4-pyridyl ring. On the other hand, close values of E_{int} were determined for the two complexes, 21.65 ± 4.96 kcal/mol (*P*) and 23.59 ± 3.62 kcal/mol (*M*). Therefore, the calculated models appeared consistent with the absence of enantiodifferentiation observed experimentally for **1c** on CDMPC.

iii) in the case of ADMPC, the calculated EEO (*P*-*M*) is consistent with the experimental elution sequence. Indeed, the following values of E_{int} were calculated for the two complexes, 41.22 ± 3.70 kcal/mol and 44.86 ± 1.92 kcal/mol for the (*P*)- and (*M*)-complexes, respectively. The two enantiomers were accommodated in two different cavities of the amylose-based nonamer. In both **1c**/ADMPC complexes, 4-hydroxyphenyl and 4-pyridyl groups protruded deeply inside the groove, with the hydroxyl group of the (*P*)-enantiomer engaged in a weak HB with the carbamate site of the selector (d = 3.290 Å), and the 4-pyridyl nitrogen of both enantiomers involved in HBs with the amidic proton of the carbamate region (d = 2.285 Å (*P*) and 2.013 Å (*M*)). More importantly, both enantiomers appeared to be buried into hydrophobic cavities generated by the nonpolar regions of the polymer (Fig. 5). This profile is in accordance with the high retention of both enantiomers of **1c** on the ADMPC (t_R (*P*) = 49.18 min, t_R (*M*) = 60.74 min), and with the hydrophobic model based on the thermodynamic analysis.

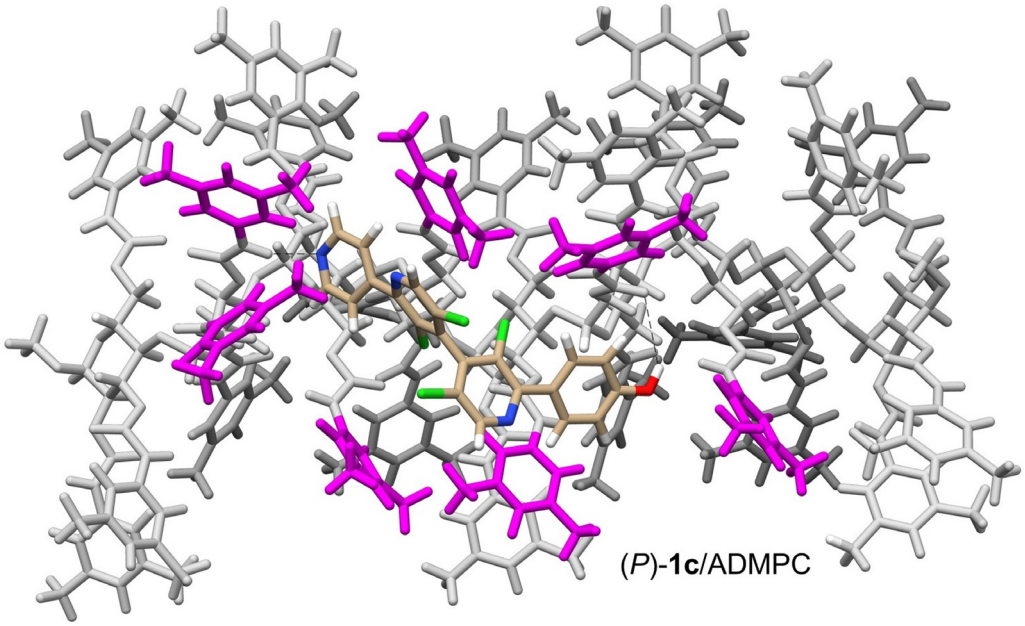

Fig. 5. Representative snapshot from the simulated MD trajectories (100 ns) of (*P*)–**1c** complex with ADMPC (solvent box, Hex/2-PrOH 90:10): tube model of the (*P*)–**1c**/ADMPC complex (legend colours: blue, nitrogen; green, chlorine; red, oxygen; white, hydrogen; magenta, aromatic rings featuring and delimiting the hydrophobic binding cavity of ADMPC (gray) hosting (*P*)–**1c** as a selectand).

4. Conclusions

While ADMPC and CDMPC showed to be complementary for the baseline enantioseparation of compounds **1a** (α_{ADMPC} = 1.26 > α_{CDMPC} = 1.14) and **1b** (α_{ADMPC} = 1.04 < α_{CDMPC} = 2.83) containing the 4-hydrophenyl and the 4-pyridyl groups, respectively, amylose-based selectors proved to be more versatile for the enantioseparation of both 4,4′-bipyridines **1c** (α_{ADMPC} = 1.25 > α_{CDMPC} = 1.00) and **1d** (α_{ADMPC} = 1.50 > α_{CDMPC} = 1.00) than cellulose-based CSPs. In particular, the enantioseparation of compound **1c** requires the use of higher concentration of alcoholic additives to shorten elution time. For instance, while elution times higher than 50 min (t_1 = 41.46 min, t_2 = 52.99 min) are needed for the enantioseparation of **1c** on iA-3 with Hex/2-PrOH 90:10 v/v as a MP (*FR* = 0.8 ml/min), the use of the mixture Hex/2-PrOH 85:15 v/v (*FR* = 1.0 ml/min) shortens elution time to 21 min (t_1 = 16.63 min, t_2 = 20.82 min).

From the mechanistic point of view, the comparison of chromatographic responses and thermodynamic profiles of compounds **1a** and **1b**, containing two different distinctive substituents, 4-hydroxyphenyl and 4-pyridyl, respectively, and compound **1c**, containing both groups, allowed for exploring the joint function of the two descriptors when located on the same scaffold. The results of this study confirmed that multisite frameworks containing both HB sites and π-extended regions can behave in multiple manner in terms of interaction ability. In compound **1c**, the co-presence of the two groups at the 2,2′-positions showed to be detrimental for enantioseparation on C-1, and in general mechanism controlled by HBs acting at the 2,2′-positions of the heteroaromatic scaffold are not very effective in terms of selectivity. Otherwise, the two groups tend to act cooperatively on amylose-based selectors through a mechanism driven by hydrophobic interactions. MD simulations confirmed that the extended π-electronic cloud of **1c** can be well accommodated in the hydrophobic cavities of the ADMPC, profiling a mechanistic picture which appears consistent with the entropic-driven feature of this enantioseparation on the amylose-based selectors.

Declaration of Competing Interest

The authors declare that they have no known competing financial interests or personal relationships that could have appeared to influence the work reported in this paper.

CRediT authorship contribution statement

Roberto Dallocchio: Investigation, Formal analysis. **Alessandro Dessì:** Investigation, Formal analysis. **Barbara Sechi:** Investigation, Data curation. **Bezhan Chankvetadze:** Resources, Writing – review & editing. **Sergio Cossu:** Resources, Writing – review & editing. **Victor Mamane:** Conceptualization, Investigation, Funding acquisition, Writing – review & editing. **Emmanuel Aubert:** Investigation, Formal analysis, Writing – review & editing. **Carla Rozzo:** Investigation, Writing – review & editing. **Giuseppe Palmieri:** Investigation, Writing – review & editing. **Ylenia Spissu:** Investigation, Writing – review & editing. **Paola Peluso:** Project administration, Conceptualization, Funding acquisition, Writing – original draft.

Acknowledgements

We thank CNR, University of Strasbourg and CNRS for financial support. The EXPLOR mesocenter is thanked for providing access to their computing facility (project 2019CPMXX0984/wbg13).

Supplementary materials

Supplementary material associated with this article can be found, in the online version, at doi:10.1016/j.jcoa.2022.100030.

References

[1] B. Chankvetadze, Recent developments on polysaccharide-based chiral stationary phases for liquid-phase separation of enantiomers, J Chromatogr A 1269 (2012) 26–51. https://doi.org10.1016/j.chroma.2012.10.033.

[2] P. Peluso, V. Mamane, R. Dallocchio, A. Dessì, S. Cossu, Noncovalent interactions in high-performance liquid chromatography enantioseparations on polysaccharide-based chiral selectors, J Chromatogr A 1623 (2020) 461202. https://doi.org10.1016/j.chroma.2020.461202.

[3] B. Chankvetadze, Recent trends in preparation, investigation and application of polysaccharide-based chiral stationary phases for separation of enantiomers in high-performance liquid chromatography, Trends Anal Chem 122 (2020) 115709. https://doi.org10.1016/j.trac.2019.115709.

[4] R. Weiss, E. Aubert, P. Peluso, S. Cossu, P. Pale, V. Mamane, Chiral chalcogen bond donors based on the 4,4'-bipyridine scaffold, Molecules 24 (2019) 4484. https://doi.org10.3390/molecules24244484.

[5] P. Peluso, V. Mamane, E. Aubert, A. Dessì, R. Dallocchio, A. Dore, et al., Insights into halogen bond-driven enantioseparations, J Chromatogr A 1467 (2016) 228–238. https://doi.org10.1016/j.chroma.2016.06.007.

[6] P. Peluso, V. Mamane, R. Dallocchio, A. Dessì, R. Villano, D. Sanna, et al., Polysaccharide-based chiral stationary phases as halogen bond acceptors: a novel strategy for detection of stereoselective σ-hole bonds in solution, J Sep Sci 41 (2018) 1247–1256. https://doi.org10.1002/jssc.201701206.

[7] R. Dallocchio, A. Dessì, M. Solinas, A. Arras, S. Cossu, E. Aubert, et al., Halogen bond in high-performance liquid chromatography enantioseparations: description, features and modelling, J Chromatogr A 1563 (2018) 71–81. https://doi.org10.1016/j.chroma.2018.05.061.

[8] A. Rang, M. Engeser, N.M. Maier, M. Nieger, W. Lindner, C.A. Schalley, Synthesis of axially chiral 4,4'-bipyridines and their remarkably selective self-assembly into chiral metallo-supramolecular squares, Chem Eur J 14 (2008) 3855–3859. https://doi.org10.1002/chem.200800113.

[9] E. Aubert, M. Abboud, A. Doudouh, P. Durand, P. Peluso, A. Ligresti, B. Vigolo, S. Cossu, P. Pale, V. Mamane, Silver(I) coordination polymers with 3,3',5,5'-tetrasubstituted 4,4'-bipyridine ligands: towards new porous chiral materials, RSC Adv 7 (2017) 7358–7367. https://doi.org10.1039/C6RA28197D.

[10] C. Gatti, A. Dessì, R. Dallocchio, V. Mamane, S. Cossu, R. Weiss, P. Pale, E. Aubert, P. Peluso, Factors impacting σ- and π-hole regions as revealed by the electrostatic potential and its source function reconstruction: the case of 4,4'-bipyridine derivatives, Molecules 25 (2020) 4409. https://doi.org10.3390/molecules25194409.

[11] P. Peluso, B. Sechi, G. Lai, A. Dessì, R. Dallocchio, S. Cossu, et al., Comparative enantioseparation of chiral 4,4'-bipyridine derivatives on coated and immobilized amylose-based chiral stationary phases, J Chromatogr A 1625 (2020) 461303. https://doi.org10.1016/j.chroma.2020.461303.

[12] R. Dallocchio, B. Sechi, A. Dessì, B. Chankvetadze, S. Cossu, V. Mamane, P. Pale, P. Peluso, Enantioseparations of polyhalogenated 4,4'-bipyridines on polysaccharide-based chiral stationary phases and molecular dynamics simulations of selector–selectand interactions, Electrophoresis 42 (2021) 1853–1863. https://doi.org10.1002/elps.202100049.

[13] A. Dessì, P. Peluso, R. Dallocchio, R. Weiss, G. Andreotti, M. Allocca, E. Aubert, P. Pale, V. Mamane, S. Cossu, Rational design, synthesis, characterization and evaluation of iodinated 4,4'-bipyridines as new transthyretin fibrillogenesis inhibitors, Molecules 25 (2020) 2213. https://doi.org10.3390/molecules25092213.

[14] P. Peluso, V. Mamane, G. Palmieri, C. Rozzo, Y. Spissu (2021) *unpublished results*.

[15] E. Aubert, E. Wenger, P. Peluso, V. Mamane, Convenient access to functionalized non-symmetrical atropisomeric 4,4'-bipyridines, Compounds 1 (2021) 58–74. https://doi.org10.3390/compounds1020006.

[16] H. Koller, K.–E. Rimböck, A. Mannschreck, High-pressure liquid chromatography on triacetylcellulose: characterization of a sorbent for the separation of enantiomers, J Chromatogr A 282 (1983) 89–94. https://doi.org10.1016/S0021-9673(00)91594-2.

[17] Y. Shao, L.F. Molnar, Y. Jung, J. Kussmann, C. Ochsenfeld, S.T. Brown, et al., Advances in methods and algorithms in a modern quantum chemistry program package, Phys Chem Chem Phys 8 (2006) 3172–3191. https://doi.org10.1039/B517914A.

[18] M.J. Frisch, G.W. Trucks, H.B. Schlegel, G.E. Scuseria, M.A. Robb, J.R. Cheeseman, G. Scalmani, V. Barone, B. Mennucci, G.A. Petersson, H. Nakatsuji, M. Caricato, X. Hratchian, H.P. Li, A.F. Izmaylov, J. Bloino, G. Zheng, J.L. Sonnenberg, M. Hada, M. Ehara, K. Toyota, R. Fukuda, J. Hasegawa, M. Ishida, T. Nakajima, Y. Honda, O. Kitao, H. Nakai, T. Vreven, J.A. Montgomery Jr., J.E. Peralta, F. Ogliaro, M. Bearpark, J.J. Heyd, E. Brothers, K.N. Kudin, V.N. Staroverov, T. Keith, R. Kobayashi, J. Normand, K. Raghavachari, A. Rendell, J.C. Burant, S.S. Iyengar, J. Tomasi, M. Cossi, N. Rega, J.M. Millam, M. Klene, J.E. Knox, J.B. Cross, V. Bakken, C. Adamo, J. Jaramillo, R. Gomperts, R.E. Stratmann, O. Yazyev, A.J. Austin, R. Cammi, C. Pomelli, J.W. Ochterski, R.L. Martin, R.L. Morokuma, V.G. Zakrzewski, G. Voth, P. Salvador, J.J. Dannenberg, S. Dapprich, A.D. Daniels, O. Farkas, J.B. Foresman, J. Ortiz, J. Cioslowski, D.J. Fox, Gaussian 09, revision B.01, Gaussian Inc., Wallingford CT, USA, 2010.

[19] T. Lu, F. Chen, Multiwfn: a multifunctional wavefunction analyzer, J Comput Chem 33 (2012) 580–592. https://doi.org10.1002/jcc.22885.

[20] T. Lu, F. Chen, Quantitative analysis of molecular surface based on improved marching tetrahedra algorithm, J Mol Graph Model 38 (2012) 314–323. https://doi.org10.1016/j.jmgm.2012.07.004.

[21] D.A. Case, I.Y. Ben-Shalom, S.R. Brozell, D.S. Cerutti, T.E. Cheatham III, V.W.D. Cruzeiro, T.A. Darden, R.E. Duke, D. Ghoreishi, M.K. Gilson, H. Gohlke, A.W. Goetz, D. Greene, R. Harris, N. Homeyer, Y. Huang, S. Izadi, A. Kovalenko, T. Kurtzman, T.S. Lee, S. LeGrand, P. Li, C. Lin, J. Liu, T. Luchko, R. Luo, D.J. Mermelstein, K.M. Merz, Y. Miao, G. Monard, C. Nguyen, H. Nguyen, I. Omelyan, A. Onufriev, F. Pan, R. Qi, D.R. Roe, A. Roitberg, C. Sagui, S. Schott-Verdugo, J. Shen, C.L. Simmerling, J. Smith, R. Salomon-Ferrer, J. Swails, R.C. Walker, J. Wang, H. Wei, R.M. Wolf, X. Wu, L. Xiao, D.M. York, P.A. Kollman, AMBER 2018, University of California, San Francisco, 2018.

[22] E.F. Pettersen, T.D. Goddard, C.C. Huang, G.S. Couch, D.M. Greenblatt, E.C. Meng, et al., UCSF Chimera—A visualization system for exploratory research and analysis, J Comput Chem 25 (2004) 1605–1612. https://doi.org10.1002/jcc.20084.

[23] Y. Yamada, K. Ohyama, G. Onodera, M. Kuriyama, N. Kishikawa, N. Kuroda, Molecular-shape selectivity by naphthalimido-modified silica stationary phases: insight into the substituents effect of naphthalene on shape recognition and π–π interactions via electrostatic potential, J Chromatogr A 1425 (2015) 173–179. https://doi.org10.1016/j.chroma.2015.11.030.

[24] P. Peluso, B. Chankvetadze, The molecular bases of chiral recognition in 2-(benzylsulfinyl)benzamide enantioseparation, Anal Chim Acta 1141 (2021) 194–205. https://doi.org10.1016/j.aca.2020.10.050.

[25] B. Chankvetadze, E. Yashima, Y. Okamoto, Chloromethylphenylcarbamate derivatives of cellulose as chiral stationary phases for high-performance liquid chromatography, J Chromatogr A 670 (1994) 39–49. https://doi.org10.1016/0021-9673(94)80278-5.

[26] B. Chankvetadze, E. Yashima, Y. Okamoto, Dimethyl-, dichloro- and chloromethylphenylcarbamates of amylose as chiral stationary phases for high-performance liquid chromatography, J Chromatogr A 694 (1995) 101–109. https://doi.org10.1016/0021-9673(94)00729-S.

[27] M. Maisuradze, G. Sheklashvili, A. Chokheli, I. Matarashvili, T. Gogatishvili, T. Farkas, et al., Chromatographic and thermodynamic comparison of amylose tris(3-chloro-5-methylphenylcarbamate) coated or covalently immobilized on silica in high-performance liquid chromatographic separation of the enantiomers of select chiral weak acids, J Chromatogr A 1602 (2019) 228–236. https://doi.org10.1016/j.chroma.2019.05.026.

[28] R. Ferretti, A. Mai, B. Gallinella, L. Zanitti, S. Valente, R. Cirilli, Application of 3 μm particle-based amylose-derived chiral stationary phases for the enantioseparation of potential histone deacetylase inhibitors, J Chromatogr A 1218 (2011) 8394–8398. https://doi.org10.1016/j.chroma.2011.09.052.

[29] T. O'Brien, L. Crocker, T. Thompson, K. Thompson, P.H. Toma, D.A. Conlon, et al., Mechanistic aspects of chiral discrimination on modified cellulose, Anal Chem 69 (1997) 1999–2007. https://doi.org10.1021/ac961241l.

[30] C. Panella, R. Ferretti, A. Casulli, R. Cirilli, Temperature and eluent composition effects on enantiomer separation of carvedilol by high-performance liquid chromatography on immobilized amylose-based chiral stationary phases, J Pharm Anal 9 (2019) 324–331. https://doi.org10.1016/j.jpha.2019.04.002.

[31] I. Matarashvili, G. Kobidze, A. Chelidze, G. Dolidze, N. Beridze, G. Jibuti, et al., The effect of temperature on the separation of enantiomers with coated and covalently immobilized polysaccharide-based chiral stationary phases, J Chromatogr A 1599 (2019) 172–179. https://doi.org10.1016/j.chroma.2019.04.024.

[32] T. Fornstedt, P. Sajonz, G. Guiochon, Thermodynamic study of an unusual chiral separation. Propranolol enantiomers on an immobilized cellulase, J Am Chem Soc 119 (1997) 1254–1264. https://doi.org10.1021/ja9631458.

[33] T. Fornstedt, P. Sajonz, G. Guiochon, A closer study of chiral retention mechanisms, Chirality 10 (1998) 375–381. https://doi.org10.1002/(SICI)1520-636X(1998)10:5⟨375::AID-CHIR3⟩3.0.CO;2-5.

[34] S. Wan, R.C. Sinclair, P.V. Coveney, Uncertainty quantification in classical molecular dynamics, Phil Trans R Soc A 379 (2021) 20200082. https://doi.org10.1098/rsta.2020.0082.